JOURNAL OF GEOPHYSICAL RESEARCH, VOL. 107, NO. D12, 4151, 10.1029/2001JD000840, 2002

Global distributions of effective cloud fraction and cloud top pressure derived from oxygen A band spectra measured by the Global Ozone Monitoring Experiment: Comparison to ISCCP data

R. B. A. Koelemeijer[1] and P. Stammes
Royal Netherlands Meteorological Institute, De Bilt, Netherlands

J. W. Hovenier[2] and J. F. de Haan[3]
Department of Physics and Astronomy, Free University, Amsterdam, Netherlands

Received 17 May 2001; revised 26 October 2001; accepted 1 November 2001; published 25 June 2002.

[1] Satellite measurements of the Earth's reflected sunlight in the oxygen A band around 761 nm, as measured by the Global Ozone Monitoring Experiment (GOME) on board ERS-2, have been analyzed to obtain global distributions of effective cloud fraction and cloud top pressure for July 1995 and January 1997. These quantities have been compared to effective cloud fractions and cloud top pressures derived by the International Satellite Cloud Climatology Project (ISCCP D2), averaged over the July and January months from 1989 to 1993. We have found a reasonable agreement between the GOME O_2 A band cloud results and the climatological ISCCP D2 data. The global monthly average difference in effective cloud fraction is 0.01 for July and vanishes for January; the standard deviation of the difference is 0.10 for both months (absolute values). These effective cloud fractions hold under the assumption of optically thick clouds and are typically 2 times smaller than the real cloud fractions. The global monthly average difference in cloud top pressure is 27 hPa (July) and 36 hPa (January); the standard deviation of the difference is 110 hPa (July) and 104 hPa (January). Largest differences are found over land surfaces. *INDEX TERMS:* 0320 Atmospheric Composition and Structure: Cloud physics and chemistry; 0340 Atmospheric Composition and Structure: Middle atmosphere—composition and chemistry; 0365 Atmospheric Composition and Structure: Troposphere—composition and chemistry; 3360 Meteorology and Atmospheric Dynamics: Remote sensing; *KEYWORDS:* cloud top pressure, oxygen A band, GOME, ISCCP

1. Introduction

[2] Various techniques exist to determine cloud top height from space measurements, such as lidar [*Winker and Trepte*, 1998], as well as a number of passive methods, which, for example, make use of information contained in thermal infrared radiances [e.g., *Smith and Platt*, 1978; *Stowe et al.*, 1989; *Rossow and Schiffer*, 1999], employ the depth of the oxygen A band [e.g., *Fischer and Grassl*, 1991; *O'Brien and Mitchell*, 1992], make use of stereoscopy [*Prata and Turner*, 1997], exploit the strength of the ring effect [*Joiner and Bhartia*, 1995], or employ polarization of light scattered by molecules above the cloud deck [*Knibbe et al.*, 2000]. At present, the most common method to obtain cloud top height information from satellites employs measured thermal infrared radiances, which are converted to cloud top height or pressure using an atmospheric temperature profile that is known or assumed from another source. For example, this method is used by the International Satellite Cloud Climatology Project (ISCCP) [*Rossow and Schiffer*, 1999]. Cloud top pressures determined from the thermal infrared are sensitive to the assumed temperature profile. In this paper we make use of the oxygen A band method, which has the advantage that the retrieved cloud top pressures are insensitive to the assumed temperature profile [*O'Brien and Mitchell*, 1992; *Bréon and Bouffiès*, 1996]. The principle of the oxygen A band method is that the depth of the O_2 A band depends on the amount of O_2 above the cloud deck, and, since O_2 is a well-mixed gas, the pressure at the top of the cloud deck can be derived. Since the first space-based retrievals with the O_2 A band method [*Saiedy et al.*, 1967], aircraft experiments as well as theoretical studies have been performed [e.g., *Fischer and Grassl*, 1991; *O'Brien and Mitchell*, 1992; *Kuze and Chance*, 1994]. These studies conclude that accurate retrievals of cloud top pressure are feasible in principle, the main problems being the treatment of multiple scattering and

[1]Now at National Institute of Public Health and the Environment, Bilthoven, Netherlands.
[2]Also at Astronomical Institute "Anton Pannekoek," University of Amsterdam, Amsterdam, Netherlands.
[3]Also at Royal Netherlands Meteorological Institute, De Bilt, Netherlands.

0148-0227/02/2001JD000840$09.00

absorption inside clouds, uncertainties in the surface albedo, and instrumental spectral resolution limitations. The O_2 A band method received new attention through measurements of the Global Ozone Monitoring Experiment (GOME) [*Burrows et al.*, 1999] and POLDER [*Vanbauce et al.*, 1998] satellite instruments.

[3] GOME is a grating spectrometer covering the spectral range 237–794 nm with a resolution of 0.2–0.4 nm. The primary goal of GOME is to measure trace gas column densities in the Earth's atmosphere, most notably O_3 and NO_2. Because of the large pixel size of GOME, which can be selected to be 40 × 80 km^2 or 40 × 320 km^2, GOME pixels are often partly covered by clouds. Clouds influence the depth of gaseous absorption lines, particularly if the trace gas concentration is high in the troposphere. Therefore, for accurate trace gas column density retrievals, the presence of clouds must be taken into account. This can be done by exploiting cloud properties derived from the O_2 A band measurements from GOME. The most important cloud parameters needed to correct trace gas column density retrievals for the presence of clouds are cloud fraction, cloud optical thickness, and cloud top pressure [*Koelemeijer and Stammes*, 1999a]. However, it is almost impossible to derive uniquely both cloud fraction and cloud optical thickness from the measured spectral reflectivity of a single GOME pixel. This is because cloudy scenes with the same cloud top pressure may possess different cloud fractions and cloud optical thicknesses which give rise to nearly the same reflectivity in and around the oxygen A band. For cloudy scenes differing in this sense, however, cloud effects on the ozone column density retrieval are almost the same [*Koelemeijer and Stammes*, 1999b]. Therefore it is useful and necessary to introduce an effective cloud fraction, which is the cloud fraction derived from the satellite measurements, assuming an a priori chosen cloud optical thickness or cloud albedo (see section 2.2). Then, the most relevant cloud parameters for trace gas column density retrieval reduce to effective cloud fraction and cloud top pressure.

[4] The current record of GOME ozone data has been processed using effective cloud fractions derived by the Initial Cloud Fitting Algorithm (ICFA) [*Deutsches Zentrum für Luft- und Raumfahrt* (*DLR*), 1994] and cloud top pressures taken from the ISCCP climatology [*Rossow et al*, 1993; *Rossow and Schiffer*, 1999]. However, considerable errors of 0.2 ± 0.2 are present in the ICFA effective cloud fractions, and the actual cloud top pressure may differ significantly from the climatological mean value [*Koelemeijer and Stammes*, 1999c]. Therefore, in an earlier paper, we have described an improved cloud retrieval method, called Fast Retrieval Scheme for Clouds from the Oxygen A Band (FRESCO), to derive effective cloud fraction and cloud top pressure simultaneously from the GOME measurements in and around the O_2 A band [*Koelemeijer et al.*, 2001] (hereinafter referred to as paper 1). In that paper, a sensitivity study was performed regarding the main assumptions in our retrieval method. In addition, we compared the cloud parameters derived using FRESCO with corresponding quantities derived from colocated Along Track Scanning Radiometer 2 (ATSR-2) measurements over Europe, but only for a few hundreds of GOME pixels. This showed an average difference (FRESCO - ATSR-2) in effective cloud fraction of 0.04 (standard deviation 0.09) and in cloud top pressure of 65 hPa (standard deviation 92 hPa). The aims of the present paper are (1) to validate the FRESCO monthly average cloud parameters globally by comparing them to monthly average values from the ISCCP climatology and (2) to provide the first global distributions of cloud top pressure derived from GOME measurements of the O_2 A band.

2. Retrieval Method

2.1. Overview of FRESCO

[5] The FRESCO method is described in detail in paper 1; here a brief overview is given. Figure 1 shows normalized reflectivities measured by GOME for a cloud-free and a cloudy scene over the Atlantic Ocean. For this figure the reflectivities were normalized to unity at 758 nm (in the continuum), to compare the shapes of the spectra; at 758 nm the reflectivities are 0.053 and 0.84 for the two scenes. Here, the reflectivity is defined as π times the Earth's reflected radiance divided by the incident solar irradiance at the top of the atmosphere through a horizontal surface unit. Clearly, the O_2 A band is less deep for the cloudy scene, because of screening of O_2 inside and below the cloud. Therefore the depth of the band provides information on cloud top pressure, whereas the reflectivity in the continuum provides information on the effective cloud fraction.

[6] Our retrieval method is based on minimizing the difference between a measured and a simulated spectrum. To simulate the spectrum of a partly cloudy pixel, a simple atmospheric transmission model is used, in which the atmosphere above the ground surface (for the clear part of the pixel) or cloud (for the cloudy part of the pixel) is treated as a purely absorbing, nonscattering, medium. Reflection occurs only at the surface or cloud top, which are both assumed to be Lambertian reflectors. The reflectivity $R(\lambda, \theta, \theta_0)$ at a wavelength λ, for a viewing zenith angle θ and a solar zenith angle θ_0, is then given by

$$R(\lambda,\theta,\theta_0) = (1-c)\,T(\lambda,P_s,\theta,\theta_0)A_s + cT(\lambda,P_s,\theta,\theta_0)A_c, \quad (1)$$

where c is the effective cloud fraction, P_s is the surface pressure, A_s is the surface albedo, P_c is the cloud top pressure, and A_c is the cloud albedo. $T(\lambda, P, \theta, \theta_0)$ is the direct atmospheric transmittance for light entering the atmosphere from the solar direction, propagating down to pressure level P and then propagating to the top of the atmosphere in the direction of the satellite. The transmittance calculations were performed in two steps. First, based on spectroscopic parameters from the 1996 high-resolution transmission molecular absorption database (HITRAN'96) [*Gamache et al.*, 1998], oxygen A band absorption cross sections were calculated, which yielded line-by-line transmittances. Second, the line-by-line transmittances were convoluted with the GOME slit function. Temperature and pressure profiles were assumed for a midlatitude summer atmosphere [*Anderson et al.*, 1986].

[7] The surface albedo, the cloud albedo, and the surface pressure have been chosen a priori. The surface albedo is fixed to 0.02 for ocean. For land it is deduced from a global minimum reflectivity database which we generated from two months of GOME data (a January and a July month) at a wavelength of 758 nm. The minimum of both

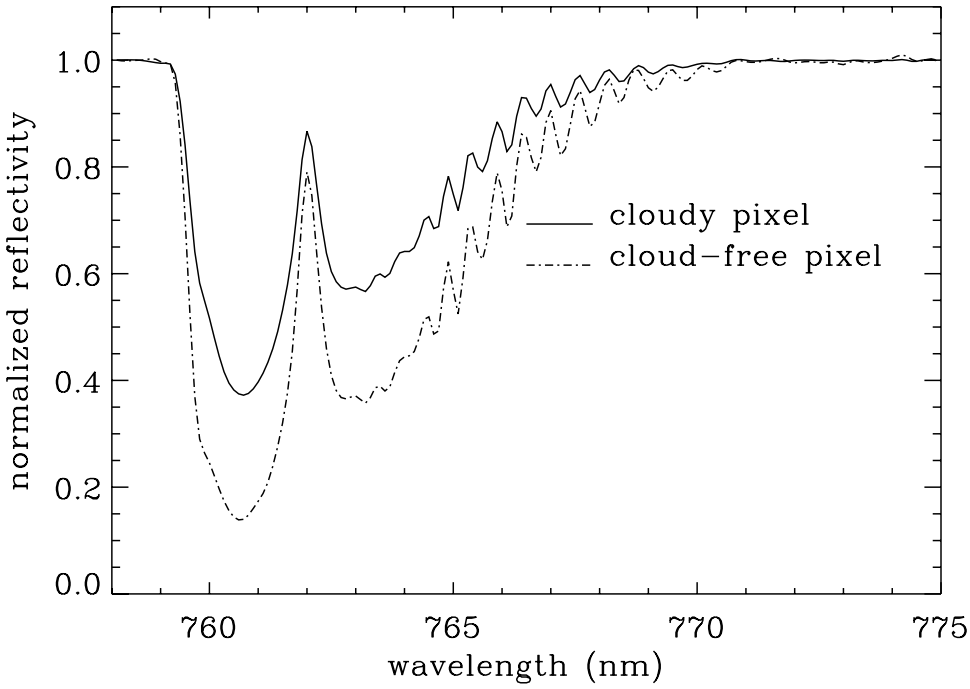

Figure 1. Two spectra of the O_2A band (cloud-free and cloudy), measured by GOME on 4 September 1998 over the Atlantic Ocean, with comparable viewing and illumination angles. The spectral resolution at these wavelengths is about 0.4 nm; the spectral sampling is about 0.2 nm. The ground pixel size is 40 × 320 km^2.

months is taken; that is, seasonal variation of the surface albedo is not (yet) taken into account. We have chosen a fixed cloud albedo of 0.8 and derive an effective cloud fraction, pertaining to an optically thick cloud (the cloud optical thickness that pertains to a spherical albedo of 0.8 is ∼33). The reasons for choosing a high cloud albedo of 0.8 are as follows. First, by choosing the rather extreme value for the cloud albedo of 0.8 the effective cloud fraction is able to span a large range of cloudy situations which occur in reality; if, for example, 0.6 were chosen, large fitting errors would occur for cases with optically thick clouds. Second, in the FRESCO method we assume that absorption below the cloud may be neglected, which can be justified for optically thick clouds. Choosing a high cloud albedo ensures that the model assumptions are internally consistent. Third, the choice A_c = 0.8 is optimized for ozone column density retrievals from GOME ultraviolet measurements; see *Koelemeijer and Stammes* [1999b]. In paper 1 it is shown that the ambiguity in cloud fraction and cloud optical thickness does not lead to significant errors in the derived cloud top pressure for most cases. In section 2.2 we show that for clouds above dark surfaces this conclusion also holds for clouds much thinner than those discussed in paper 1. This extension to thinner clouds is particularly relevant for this global comparison, because the global average cloud optical thickness is ∼4 [*Rossow and Schiffer*, 1999].

[8] The effective cloud fraction and cloud top pressure are derived by iteratively minimizing the chi-square difference between the measured and simulated reflectivity spectra. In the minimization we assume that errors in the measured and modeled reflectivities do not depend on wavelength. Furthermore, since the signal-to-noise ratio is high, we expect that the total error is not dominated by noise but by systematic errors.

2.2. Effective Cloud Fraction Concept

[9] It is almost impossible to uniquely derive both cloud fraction and cloud optical thickness for an individual pixel from the measured spectral reflectivity in and around the oxygen A band, because cloudy scenes with the same cloud top pressure but with different cloud fractions and cloud optical thicknesses may give rise to (almost) the same spectral reflectivity. To illustrate this, we performed multiple-scattering calculations in and outside the oxygen A band with a doubling-adding radiative transfer model [*de Haan et al.*, 1987; *Stammes*, 2000]. In these calculations a Rayleigh scattering midlatitude summer atmosphere was assumed, bounded by a Lambertian ground surface. Cloud layers with a geometrical thickness of 1 km and different optical thicknesses, b_c, were inserted at various heights in the atmosphere. For the cloud particles a Henyey-Greenstein phase function was assumed with an asymmetry parameter of 0.85 and a single-scattering albedo of 1. To simulate the reflectivity of a partly cloudy scene, the reflectivities of a cloud-free and fully cloudy atmosphere were added, weigh-ted with the fractional coverage of the cloud-free and cloudy parts of the pixel. Instead of performing a complete sensitivity study that would involve lengthy line-by-line calculations for all atmospheric scenarios, we have chosen to perform calculations for four oxygen absorption optical thicknesses, namely for b_{o2} = 1.62, 0.35, 0.026, and 0, which span a relevant range in oxygen (total column) optical thicknesses

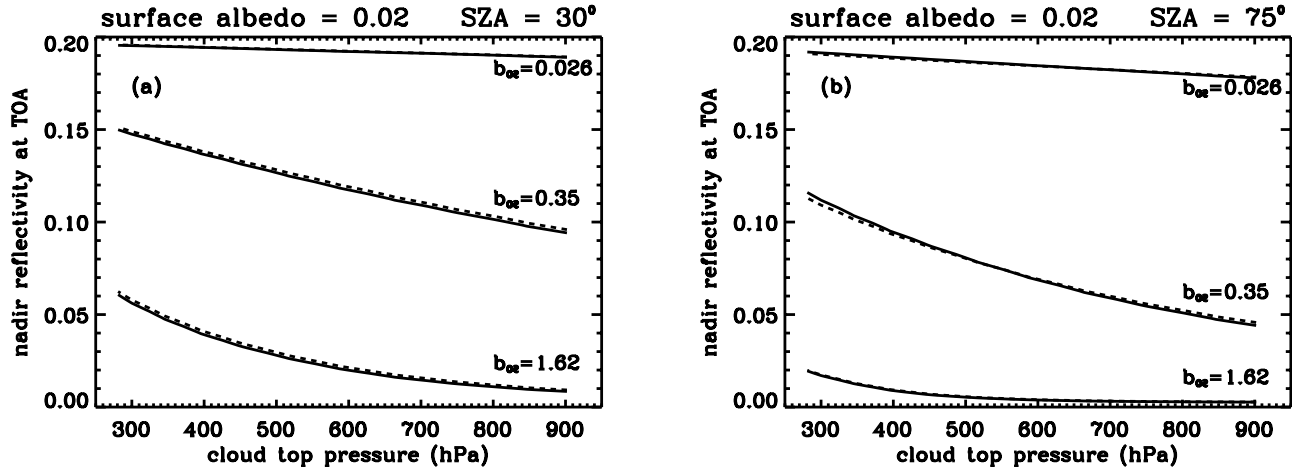

Figure 2. Calculated nadir reflectivities in the O_2 A band for cloudy scenes with different cloud fractions and cloud optical thicknesses but with the same nadir reflectivity at the top of the atmosphere (TOA) in the continuum (= 0.2), as functions of cloud top pressure. Solid curves indicate maximum cloud fraction and minimum cloud optical thickness; dashed curves indicate minimum cloud fraction and maximum cloud optical thickness. The b_c and c values corresponding to these curves are listed in Table 1 (first row). Other cloud properties are mentioned in the text (section 2.2). Results are shown for solar zenith angles (SZA) of (a) 30° and (b) 75°.

in the wavelength region 758–766 nm. This is sufficient to demonstrate the effective cloud fraction concept.

[10] We varied b_c between 0 and 100, c between 0 and 1, and P_c between 280 and 900 hPa. For each P_c value we considered cases with different values of b_c and c but with the same nadir reflectivity at the top of the atmosphere in the continuum, R_{con}. For these cases, referred to as (b_c,c)-equivalent cases, we investigated the variation in the reflectivity at absorbing wavelengths. R_{con} was varied from 0.2 to 0.8, or a smaller range if these values could not be obtained for a given scenario.

[11] Figures 2a and 2b show nadir reflectivities inside the oxygen A band as functions of cloud top pressure, for R_{con} = 0.2, A_s = 0.02, and θ_0 = 30° and 75°. In Figures 2a and 2b, different pairs of curves pertain to different oxygen absorption optical thicknesses. Within a pair the solid curve pertains to the cloudy case with maximum cloud fraction and minimum cloud optical thickness yielding R_{con} = 0.2, denoted by ($b_{c,min}$, c_{max}), and the dashed curve pertains to the cloudy case with minimum cloud fraction and maximum cloud optical thickness yielding R_{con} = 0.2, denoted by ($b_{c,max}$, c_{min}). Thus the most extreme (b_c,c)-equivalent cases are shown. Clearly, for most cloud top pressures the variation in the reflectivity inside the O_2 A band due to (b_c,c) variation is small if the reflectivity outside the O_2 A band is the same. As a consequence, simultaneous retrieval of both b_c and c from a single O_2 A band spectrum is almost impossible. However, this does not lead to large errors in the retrieved P_c in general. Table 1 shows the average cloud top pressure difference between the most extreme (b_c,c)-equivalent cases, ΔP_c. Here we averaged over all cloud top pressures, and we considered absolute values of the differences to avoid canceling of positive and negative differences. This serves as an estimate for the maximum cloud top pressure retrieval error due to ambiguity in b_c and c. Also, Table 1 presents c_{min} pertaining to b_c = 100, and $b_{c,min}$ pertaining to c = 1. Results are given for A_s = 0.02, which is representative for ocean, and for A_s = 0.3, which is representative for vegetated area. The results shown here are an extension toward smaller cloud optical thicknesses of calculations presented in paper 1. From our calculations we conclude that for surfaces with a low albedo, cloud top pressure retrieval errors due to ambiguity in b_c and c are smaller than 20 hPa. Hence P_c can be retrieved quite accurately although b_c (or A_c) is chosen a priori. For surfaces with high albedo the error increases, particularly when the reflectivity is close to the surface albedo, as can be observed in Table 1.

2.3. Results of Sensitivity Analysis

[12] In paper 1 a sensitivity study was performed regarding the main assumptions in FRESCO. Eight sensitivity experiments were described, quantifying the effects of errors

Table 1. Estimated Error in the Derived Cloud Top Pressure ΔP_c Arising From Ambiguity in Cloud Fraction and Cloud Optical Thickness[a]

		θ_0 = 30°			θ_0 = 75°		
A_s	R_{con}	ΔP_c (hPa)	$b_{c,min}$	c_{min}	ΔP_c (hPa)	$b_{c,min}$	c_{min}
0.02	0.2	16	4.5	0.18	11	2.6	0.24
0.02	0.3	14	6.6	0.29	6	5.4	0.39
0.02	0.4	11	9.1	0.40	4	9.7	0.54
0.02	0.5	9	12	0.50	3	17	0.69
0.02	0.6	7	17	0.61	2	32	0.84
0.02	0.7	6	24	0.71	1	87	0.99
0.02	0.8	4	35	0.82	–	–	–
0.30	0.4	45	5.1	0.14	122	5.9	0.24
0.30	0.5	28	8.7	0.29	58	13	0.48
0.30	0.6	16	13	0.44	26	28	0.73
0.30	0.7	12	20	0.59	2	83	0.97
0.30	0.8	8	32	0.74	–	–	–

[a]The $b_{c,min}$ values pertain to $c = c_{max} = 1$, and the c_{min} values pertain to $b_c = b_{c,max} = 100$.

in (1) wavelength calibration, (2) radiometric calibration, (3) atmospheric profile, (4) surface pressure, (5) surface albedo, (6) cloud albedo, (7) cloud anisotropic reflection, and (8) fitting method. From this, we concluded that the most notable errors in the derived c and P_c are due to errors in the assumed surface albedo and cloud albedo and due to the choice of the fitting method. Regarding uncertainties in the assumed surface albedo, we found that, assuming errors in the ocean albedo of ±0.02 and in the land albedo of ±0.05, the average absolute errors in c are 0.02 and 0.05, respectively, and the average absolute errors in P_c are 15 hPa and 53 hPa, respectively. We found that the assumed value of A_c does not influence the derived value of P_c for surfaces with low albedo, such as ocean, consistent with the results presented here; for land surfaces the choice $A_c = 0.8$ may lead to smaller P_c values (22 hPa on average) as compared to the choice $A_c = 0.6$. Whether or not assuming the radiometric error to be wavelength dependent in the fitting gives rise to an average difference of 26 hPa for P_c, for c no difference is found. The assumed temperature profile has negligible influence on the values of P_c and c derived by FRESCO, in line with results of *Bréon and Bouffiès* [1996].

3. Comparison With ISCCP-D2 Data

[13] Two months of GOME data were processed with FRESCO, namely July 1995 and January 1997. These months were selected according to two criteria: (1) Sufficient data should be available to calculate a representative monthly average, and (2) the El Niño–Southern Oscillation should not be extreme, in order to allow a meaningful comparison to climatological values.

[14] In order to better compare the effective cloud fractions of FRESCO with the cloud fractions from ISCCP the latter were converted to effective cloud fractions, by multiplying them with the ratio A_1/A_2. Here, A_1 is the spherical albedo of a cloud with the optical thickness reported in the ISCCP D2 data set (calculated for each ISCCP grid cell), and $A_2 = 0.8$ is the cloud albedo value used in FRESCO. We have chosen the spherical albedo for this conversion, because the ISCCP satellite data were acquired under many different solar and viewing geometries for the same location. The spherical albedo has been calculated off-line as a function of cloud optical thickness using the doubling-adding model described in section 2.2. We assumed a two-parameter gamma cloud droplet size distribution with an effective radius of 6 μm and an effective variance of 1/9 (the C1-cloud model of *Deirmendjian* [1969, p. 78]), and a single-scattering albedo of unity. We could not convert the FRESCO effective cloud fractions to independent values of cloud fraction and cloud optical thickness, because of lack of information on subpixel cloud variability in the GOME spectra. Globally averaged, the ratio A_1/A_2 is 0.45 for July and 0.47 for January; thus the real ISCCP cloud fractions are more than 2 times larger than the ISCCP effective cloud fractions considered in this paper. Because the ISCCP data are not yet available for the years after the launch of GOME (in 1995), we compared with January and July averages of ISCCP data, averaged over 1989–1993 (5 years).

[15] The FRESCO monthly average values of effective cloud fraction and cloud top pressure have been calculated for grid cells of 2.5° × 2.5°, corresponding to the grid size used in the ISCCP D2 data product. The maps of July 1995 are shown in Figures 3a and 3e. The corresponding quantities from the ISCCP-D2 data set averaged over the July months of 1989–1993 are shown in Figures 3b and 3e. The FRESCO method has not been used over snow/ice-covered surfaces and for solar zenith angles larger than 85°. Areas pertaining to such conditions and areas with missing data are shown in black. Figure 3c shows the zonally averaged effective cloud fractions obtained from FRESCO and ISCCP, as well as their differences. Figure 3f shows the zonally averaged cloud top pressures and their differences. Figures 4a–4f are the same as Figures 3a–3f, but for January instead of July. Clearly, as can be observed from Figures 3 and 4, there is agreement between the FRESCO and ISCCP results regarding the main global cloud features, such as low-altitude marine stratus clouds off the west coasts of continental land masses and high-altitude convective clouds in the intertropical convergence zone.

[16] For a quantitative comparison between the FRESCO and ISCCP results we calculated various averages and standard deviations of their differences, to be specified below. We compared these averages and standard deviations to the interannual variability, as estimated from the ISCCP data, and to the error in the ISCCP data. If the differences between FRESCO and ISCCP are much larger than what might be expected from interannual variability and errors in the ISCCP data, we have attributed these differences to errors in FRESCO. In the following, the symbols $\langle c\rangle$ and $\langle P_c\rangle$ are used to denote the monthly average value of effective cloud fraction and cloud top pressure in a grid cell of 2.5° × 2.5°, respectively. For various parts of the Earth, spatial averages of the $\langle c\rangle$ and $\langle P_c\rangle$ values have been calculated, denoted by $[\langle c\rangle]$ and $[\langle P_c\rangle]$. The quantities pertaining to FRESCO and ISCCP have been subscripted by F and I, respectively. The difference $\langle c\rangle_F - \langle c\rangle_I$ is denoted by $\delta_{\langle c\rangle}$; the difference $\langle P_c\rangle_F - \langle P_c\rangle_I$ is denoted by $\delta_{\langle Pc\rangle}$. Spatial averages and spatial standard deviations of the $\delta_{\langle c\rangle}$ and $\delta_{\langle Pc\rangle}$ values have been calculated for the various parts of the Earth; the average differences are denoted by $[\delta_{\langle c\rangle}]$ and $[\delta_{\langle Pc\rangle}]$, and the standard deviations are denoted by $\sigma(\delta_{\langle c\rangle})$ and $\sigma(\delta_{\langle Pc\rangle})$, respectively.

[17] We may ask what values of $[\delta_{\langle c\rangle}]$, $[\delta_{\langle Pc\rangle}]$, $\sigma(\delta_{\langle c\rangle})$, and $\sigma(\delta_{\langle Pc\rangle})$ we may expect due to the fact that cloud properties from 1 year (FRESCO) are compared to averages of other years (ISCCP). To estimate this effect of interannual variability, we calculated five maps of the difference between the monthly average values of each single year in the ISCCP data set and the mean of the 4 other years in that data set, for grid cells of 2.5° × 2.5°. These differences are denoted by $\delta^*_{\langle c\rangle}$ for the effective cloud fractions and $\delta^*_{\langle Pc\rangle}$ for the cloud top pressures. For each map, spatial averages and standard deviations have been calculated for various parts of the Earth. These results do not vary much from map to map. Therefore these spatial averages and spatial standard deviations have been averaged over the five maps to obtain a measure for the effect of interannual variability. The average differences pertaining to the interannual variability are denoted by $[\delta^*_{\langle c\rangle}]$ and $[\delta^*_{\langle Pc\rangle}]$, and the standard deviations are denoted by $\sigma(\delta^*_{\langle c\rangle})$ and $\sigma(\delta^*_{\langle Pc\rangle})$. Thus this process to estimate the effect of interannual variability resembles the procedure used in the comparison

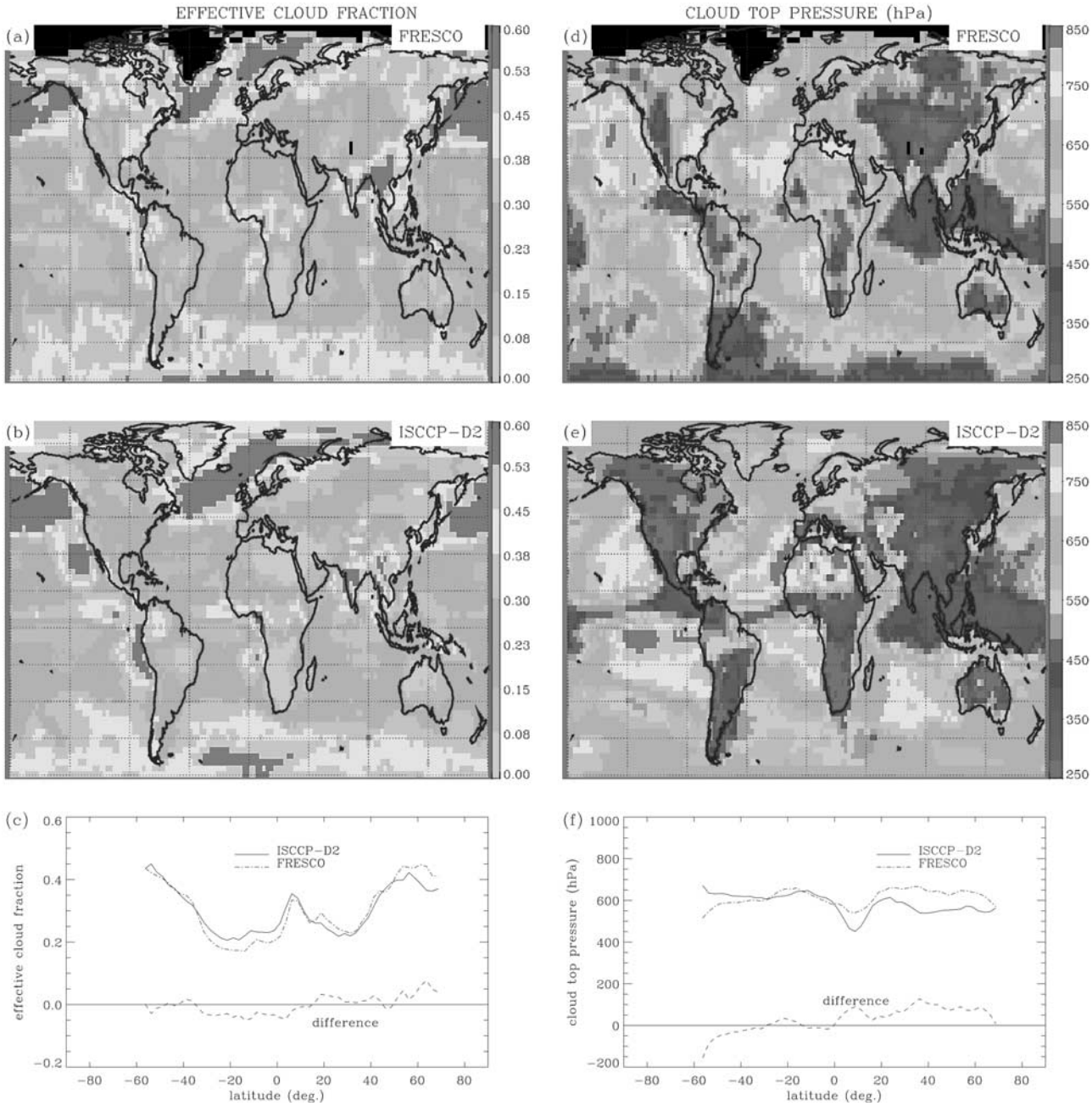

Figure 3. Monthly average effective cloud fractions and cloud top pressures of FRESCO and ISCCP. Effective cloud fractions are given for (a) FRESCO results, (b) ISCCP D2 results, and (c) zonal average; cloud top pressures (hectopascals) are given for (d) FRESCO results, (e) ISCCP results, and (f) zonal average. The FRESCO results are for July 1995, and the ISCCP results are July averages of 1989–1993. See color version of this figure at back of this issue.

between FRESCO and ISCCP data. To calculate $[\delta^*_{\langle c\rangle}]$ and $[\delta^*_{\langle Pc\rangle}]$, absolute difference values were considered, because otherwise the results for $[\delta^*_{\langle c\rangle}]$ and $[\delta^*_{\langle Pc\rangle}]$ would vanish (by definition). We also calculated spatially averaged temporal standard deviations of $\langle c\rangle_I$ and $\langle P_c\rangle_I$ based on the 5 years of ISCCP data; these standard deviations are of the same order of magnitude as the values of $\sigma(\delta^*_{\langle c\rangle})$ and $\sigma(\delta^*_{\langle Pc\rangle})$.

[18] Table 2 lists statistics of the monthly average effective cloud fractions of FRESCO and ISCCP and statistics on the interannual variability of the monthly average effective cloud fraction. The results have been presented separately for land and ocean, and for both hemispheres, and have been weighted according to the area of the grid cells. Similarly, Table 3 lists the statistics for the monthly average cloud top pressures. From histogram analysis we verified that the statistics of the difference between FRESCO and ISCCP are Gaussian, both for the effective cloud fractions and for the cloud top pressures.

[19] A detailed review of error sources in the ISCCP cloud products is given by *Rossow and Schiffer* [1999, and

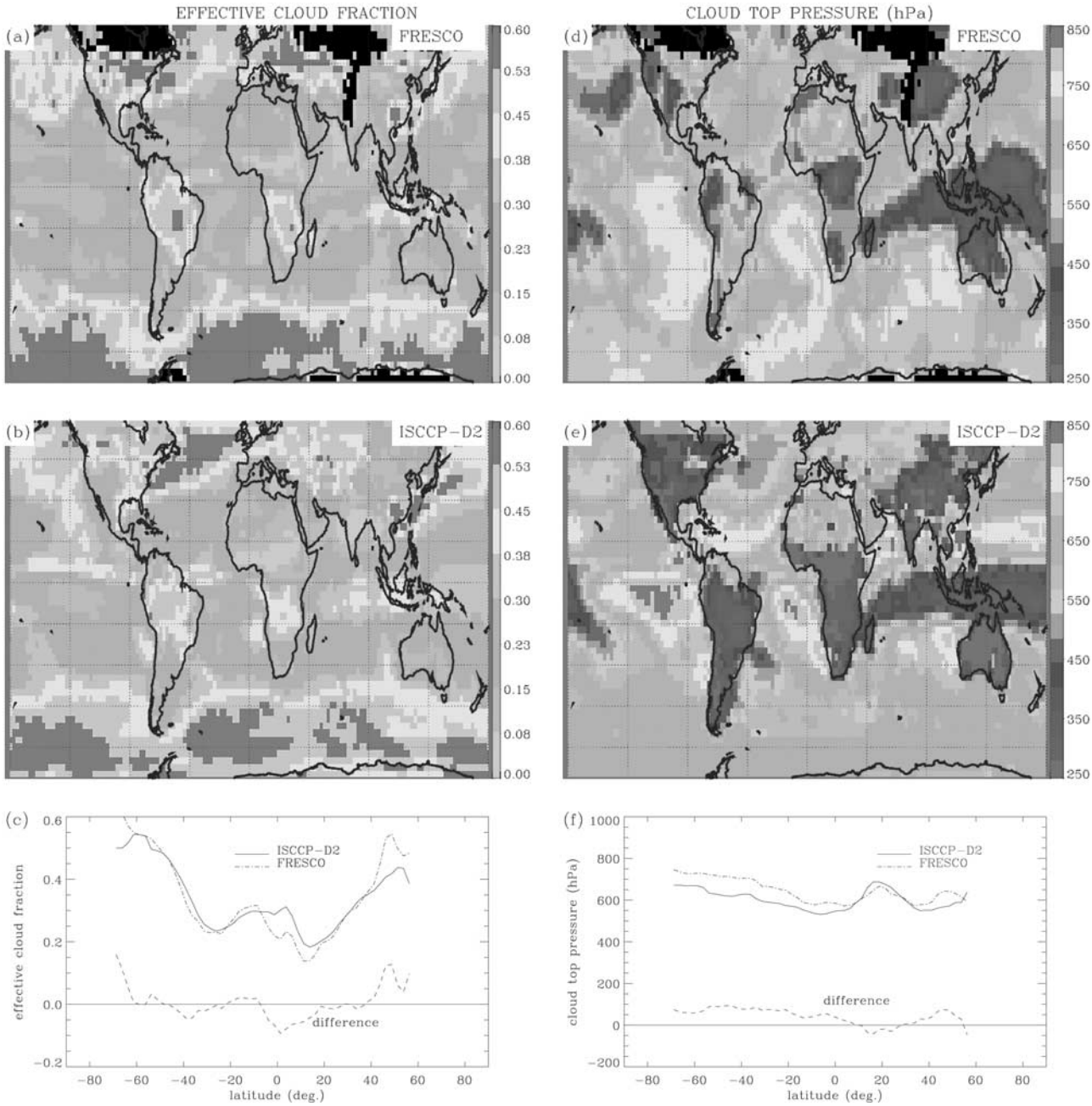

Figure 4. Same as Figure 3, but now the FRESCO results are for January 1997, and the ISCCP results are January averages of 1989–1993. See color version of this figure at back of this issue.

references therein]. Here, only a short summary of the main error sources relevant for our study is given. Comparison of ISCCP (stage D) cloud fractions to surface observations shows that the former are in excess of the latter by 0.05 both over land and over ocean, for all seasons, and for most of the globe. Cloud fraction errors are larger in the polar regions. Regarding the effective cloud fractions, which we deduced from the ISCCP cloud fraction and cloud optical thickness products, probably the largest error source is due to the limited absolute accuracy of the visible reflectances used by ISCCP, which is estimated to be ~10% [*Brest et al.*, 1997]. Therefore we estimate that the error in the effective cloud fractions deduced from ISCCP may also be about 10%, i.e., about 0.03. It is, however, important to note that the calibration error is a systematic error, independent of geographical location (although discontinuities may occur between adjacent portions of the globe viewed by different satellite instruments). Cloud top pressures are derived in ISCCP by converting cloud top temperatures to pressures using the TIROS Operational Vertical Sounder (TOVS) temperature profiles. The ISCCP cloud top temperatures have biases of 2–4 K, depending on cloud type. Errors in the TOVS temperature profiles are known to introduce additional biases in the derived cloud top pressures. Generally speaking, errors in monthly average cloud top pressures are typically of the order of 25–50 hPa for low and

midlevel clouds, and may be larger for optically thin high clouds.

3.1. Effective Cloud Fraction

[20] The global average effective cloud fraction values of FRESCO and ISCCP agree very well (see Table 2), and their difference is smaller than the estimated error of 0.03 in the ISCCP effective cloud fractions. For both FRESCO and ISCCP the global average effective cloud fraction is slightly higher in January than in July. Also, both data sets report more clouds in the summer hemisphere than in the winter hemisphere, and more clouds over ocean than over land. However, the land-ocean difference is larger in absolute value for ISCCP than for FRESCO. The largest differences between FRESCO and ISCCP are over the Sahara desert in both months, and over land areas in Europe and North America in January 1997, when large areas were covered by snow. Globally averaged, the standard deviation related to interannual variability is 50% (July) to 70% (January) of the standard deviation of the effective cloud fraction difference between FRESCO and ISCCP. The standard deviation of the effective cloud fraction difference is slightly smaller for clouds over ocean than for clouds over land, and the value over ocean is closer to that expected from interannual variability. This indicates that the agreement between $\langle c \rangle_I$ and $\langle c \rangle_F$ is better over ocean than over land. The reason why the discrepancy between $\langle c \rangle_I$ and $\langle c \rangle_F$ is larger than expected from interannual variability and errors in ISCCP is probably that the albedo of land is generally chosen too low in our analysis, leading to an overestimate of the effective cloud fraction in FRESCO.

3.2. Cloud Top Pressure

[21] The global maps of cloud top pressure from FRESCO and ISCCP correlate reasonably well. For both FRESCO and ISCCP the cloud top pressure is higher over ocean than over land (see Table 3). However, the cloud top pressure difference between land and ocean is much more pronounced in ISCCP than in FRESCO. The standard deviation of the difference between $\langle P_c \rangle_F$ and $\langle P_c \rangle_I$ is much larger for clouds over land than for clouds over ocean. For clouds over land it is about 3 times larger than that expected from interannual variability. This indicates that the agreement between FRESCO and ISCCP is better for clouds over ocean than for clouds over land. Furthermore, it is apparent in Figures 3f and 4f that zonally averaged $\langle P_c \rangle_F$ values are systematically higher than the $\langle P_c \rangle_I$ values in the summer hemisphere.

[22] We can identify four reasons to explain the fact that the differences between $\langle P_c \rangle_F$ and $\langle P_c \rangle_I$ are larger than expected from interannual variability considerations and from errors in the ISCCP cloud top pressures. First, if the effective cloud fraction is overestimated by FRESCO, which occurs over land more often than over ocean, the derived cloud top pressure will be overestimated as well. The reason is that similar amounts of O_2 may be screened by high clouds with small effective cloud fraction and by low clouds with large effective cloud fraction. In particular, areas with a small effective cloud fraction and high surface albedo are sensitive to such errors. Second, clouds are more opaque at thermal infrared wavelengths used by ISCCP than at near-infrared wavelengths used by FRESCO. Consequently, the cloud top pressure values derived by FRESCO will be biased toward higher values, because absorption associated with penetration of light into the cloud is not taken into account in the FRESCO retrieval model. Third, differences between the assumed and real cloud albedos may give rise to errors in the derived cloud top pressure, particularly for clouds above surfaces with high albedo, as explained in section 2.2. Fourth, diurnal variations may explain part of the differences between FRESCO and ISCCP cloud top pressures. The FRESCO results are acquired in the morning (GOME crosses the equator at 1030 local solar time), whereas the ISCCP results are 24 hour averages. Above ocean, cloud fractions are near their 24 hour average value near the time of the GOME overpass, both for low- and high-altitude clouds. Over land, however, high clouds are less frequent, and low clouds are more frequent around the GOME overpass time [*Cairns*, 1995; *Rossow and Schiffer*, 1999].

Table 2. Statistics of Monthly Average Effective Cloud Fractions[a]

Month	Subset	$[\langle c \rangle_F]$	$[\langle c \rangle_I]$	$[\delta_{\langle c \rangle}]$	$\sigma(\delta_{\langle c \rangle})$	$[\delta^*_{\langle c \rangle}]$	$\sigma(\delta^*_{\langle c \rangle})$
July	global	0.29	0.30	−0.01	0.10	0.01	0.05
July	ocean	0.31	0.33	−0.02	0.10	0.01	0.06
July	land	0.28	0.25	0.03	0.11	0.00	0.05
July	NH	0.32	0.31	0.01	0.11	0.01	0.06
July	SH	0.26	0.28	−0.02	0.09	0.01	0.05
Jan.	global	0.32	0.32	0.00	0.10	0.01	0.07
Jan.	ocean	0.34	0.35	−0.01	0.10	0.01	0.07
Jan.	land	0.31	0.27	0.04	0.12	0.01	0.07
Jan.	NH	0.29	0.30	−0.01	0.12	0.01	0.07
Jan.	SH	0.35	0.35	0.00	0.09	0.01	0.07

[a]Symbols are as follows: $[\langle c \rangle_F]$ and $[\langle c \rangle_I]$, spatial and monthly average effective cloud fractions from FRESCO and ISCCP; $[\delta_{\langle c \rangle}]$ and $\sigma(\delta_{\langle c \rangle})$, average and standard deviation of difference in monthly average effective cloud fractions; and $[\delta^*_{\langle Pc \rangle}]$ and $\sigma(\delta^*_{\langle Pc \rangle})$, average and standard deviation due to the interannual variability of monthly average effective cloud fractions, as estimated from ISCCP. NH stands for Northern Hemisphere, and SH stands for Southern Hemisphere.

Table 3. Statistics of Monthly Average Cloud Top Pressures[a]

Month	Subset	$[\langle P_c \rangle_F]$	$[\langle P_c \rangle_I]$	$[\delta_{\langle Pc \rangle}]$	$\sigma(\delta_{\langle Pc \rangle})$	$[\delta^*_{\langle Pc \rangle}]$	$\sigma(\delta^*_{\langle Pc \rangle})$
July	global	614	587	27	110	14	53
July	ocean	631	635	−4	83	18	55
July	land	584	492	92	147	6	47
July	NH	621	553	68	119	13	52
July	SH	605	625	−20	100	16	54
Jan.	global	634	598	36	104	13	58
Jan.	ocean	657	642	15	82	17	61
Jan.	land	582	500	82	140	7	50
Jan.	NH	607	602	5	105	15	62
Jan.	SH	660	595	65	103	13	54

[a]Pressures are given in hectopascals. Symbols are as follows: $[\langle P_c \rangle_F]$ and $[\langle P_c \rangle_I]$, spatial and monthly average cloud top pressures from FRESCO and ISCCP; $[\delta_{\langle Pc \rangle}]$ and $\sigma(\delta_{\langle Pc \rangle})$, average and standard deviation of difference in monthly average cloud top pressures; and $[\delta^*_{\langle Pc \rangle}]$ and $\sigma(\delta^*_{\langle Pc \rangle})$, average and standard deviation due to the interannual variability of monthly average cloud top pressures, as estimated from ISCCP. NH stands for Northern Hemisphere, and SH stands for Southern Hemisphere.

4. Concluding Remarks

[23] We have analyzed spectra of the O_2 A band measured by GOME to derive effective cloud fractions and cloud top pressures on a global scale. These are the first global cloud top pressure distributions obtained from the O_2 A

band which have been published. Although our methrod (FRESCO) to derive effective cloud fractions and top pressures from the oxygen A band is relatively simple, the monthly average effective cloud fractions and cloud top pressures show a reasonably good agreement with the ISCCP D2 data. The FRESCO method may be improved in the future by taking into account the effect of multiple scattering on absorption by O_2 in the cloud in the forward modeling. Another improvement would be the implementation of a seasonally dependent surface albedo climatology at 758 nm, which is presently being developed at the Royal Netherlands Meteorological Institute (KNMI). The cloud top pressures retrieved from the oxygen A band are insensitive to the assumed temperature profile and thus can provide independent information on cloud top pressures as compared to the brightness temperature method of ISCCP.

[24] The FRESCO effective cloud fractions and cloud top pressures are presently being used for near-real-time ozone column density retrieval at KNMI [*Piters et al.*, 1999] (see also data available from KNMI at http://www.knmi.nl/gome_fd). Under conditions, the FRESCO source code is available from the authors upon written request. The FRESCO method may also be useful for column density and profile retrievals of ozone and other trace gases from Scanning Imaging Absorption Spectrometer for Atmospheric Cartography (SCIAMACHY) (to be launched on board Envisat in 2002) and the GOME 2 series (to be launched on board of the Metop satellites from 2005 onward). Furthermore, the monitoring of effective cloud fractions and cloud top pressures by these instruments can be a useful contribution to climate studies of clouds, as these instruments will be accurately calibrated and have smaller pixel sizes than GOME.

[25] **Acknowledgments.** We are grateful to the staff at the NASA-Langley DAAC for kindly providing the ISCCP D2 data. We thank ESA for providing the GOME data through DLR. We gratefully acknowledge comments made by two reviewers on an earlier version of this paper. Particular thanks go to T. Kurosu (Harvard-Smithsonian Center for Astrophysics) for his constructive comments on this work. Financial support for this work by the Space Research Organization Netherlands and the Netherlands Agency for Aerospace Programmes is acknowledged.

References

Anderson, G. P., S. A. Clough, F. X. Kneizys, J. H. Chetwynd, and E. P. Shettle, AFGL atmospheric constituent profiles, *Tech. Rep. AFGL-TR-86-0110*, Air Force Geophys. Lab., Hanscom AFB, Mass., 1986.

Bréon, F.-M., and S. Bouffiès, Land surface pressure estimate from measurements in the O_2 A-band, *J. Appl. Meteorol.*, *35*, 67–77, 1996.

Brest, C. L., W. B. Rossow, and M. D. Roiter, Update of radiance calibrations for ISCCP, *J. Atmos. Oceanic Technol.*, *14*, 1091–1109, 1997.

Burrows, J. P., et al., The Global Ozone Monitoring Experiment (GOME): Mission concept and first scientific results, *J. Atmos. Sci.*, *56*, 151–175, 1999.

Cairns, B., Diurnal variations of cloud from ISCCP data, *Atmos. Res.*, *37*, 133–146, 1995.

de Haan, J. F., P. B. Bosma, and J. W. Hovenier, The adding method for multiple scattering calculations of polarized light, *Astron. Astrophys.*, *183*, 371–391, 1987.

Deirmendjian, D., *Electromagnetic Scattering on Spherical Polydispersions*, 290 pp., Elsevier Sci., New York, 1969.

Deutsches Zentrum für Luft- und Raumfahrt (DLR), GOME level 1 to 2 algorithms description, *Tech. Rep. ER-TN-DLR-GO-0025*, 32 pp., Oberpfaffenhofen, Germany, 1994.

Fischer, J., and H. Grassl, Detection of cloud-top height from backscattered radiances within the oxygen A band, part 1, Theoretical study, *J. Appl. Meteorol.*, *30*, 1245–1259, 1991.

Gamache, R. R., A. Goldman, and L. S. Rothman, Improved spectral parameters for the three most abundant isotopomers of the oxygen molecule, *J. Quant. Spectrosc. Radiat. Transfer*, *59*, 495–509, 1998.

Joiner, J., and P. K. Bhartia, The determination of cloud pressures from rotational Raman scattering in satellite backscatter ultraviolet measurements, *J. Geophys. Res.*, *100*, 23,019–23,026, 1995.

Knibbe, W. J. J., J. F. de Haan, J. W. Hovenier, D. M. Stam, R. B. A. Koelemeijer, and P. Stammes, Deriving terrestrial cloud top pressure from photopolarimetry of reflected light, *J. Quant. Spectrosc. Radiat. Transfer*, *64*, 173–199, 2000.

Koelemeijer, R. B. A., and P. Stammes, Effects of clouds on ozone column retrieval from GOME UV measurements, *J. Geophys. Res.*, *104*, 8281–8294, 1999a.

Koelemeijer, R. B. A., and P. Stammes, Influence of clouds on GOME ozone retrieval, in *Proceedings of the European Symposium on Atmospheric Measurements From Space*, *ESA WPP-161*, pp. 587–592, Eur. Space Agency-Eur. Space Res. and Technol. Cent., Noordwijk, Netherlands, Jan. 1999b.

Koelemeijer, R. B. A., and P. Stammes, Validation of Global Ozone Monitoring Experiment cloud fractions relevant for accurate ozone column retrieval, *J. Geophys. Res.*, *104*, 18,801–18,814, 1999c.

Koelemeijer, R. B. A., P. Stammes, J. W. Hovenier, and J. F. de Haan, A fast method for retrieval of cloud parameters using oxygen A band measurements from GOME, *J. Geophys. Res.*, *106*, 3475–3490, 2001.

Kuze, A., and K. V. Chance, Analysis of cloud top height and cloud coverage from satellites using the O_2 A and B bands, *J. Geophys. Res.*, *99*, 14,481–14,491, 1994.

O'Brien, D. M., and R. M. Mitchell, Error estimates for retrieval of cloud-top pressure using absorption in the A band of oxygen, *J. Appl. Meteorol.*, *31*, 1179–1192, 1992.

Piters, A. J. M., P. J. M. Valks, R. B. A. Koelemeijer, and D. M. Stam, GOME ozone fast delivery and value-added products algorithm specification document, *Tech. Rep. GOFAP-KNMI-ASD-01*, 23 pp., R. Neth. Meteorol. Inst., De Bilt, Netherlands, 1999.

Prata, A. J., and P. J. Turner, Cloud-top height determination using ATSR data, *Remote Sens. Environ.*, *59*, 1–13, 1997.

Rossow, W. B., and R. A. Schiffer, Advances in understanding clouds from ISCCP, *Bull. Am. Meteorol. Soc.*, *80*, 2261–2287, 1999.

Rossow, W. B., A. W. Walker, and L. C. Garder, Comparison of ISCCP and other cloud amounts, *J. Clim.*, *6*, 2394–2418, 1993.

Saiedy, F., H. Jacobowitz, and D. Q. Wark, On cloud-top determination from Gemini-5, *J. Atmos. Sci.*, *24*, 63–69, 1967.

Smith, W. L., and C. M. R. Platt, Comparison of satellite deduced cloud top heights with indications from radiosonde and ground-based laser measurements, *J. Appl. Meteorol.*, *17*, 1796–1802, 1978.

Stammes, P., Spectral radiance modeling in the UV-visible range, in *Proceedings of the International Radiation Symposium 2000: Current Problems in Atmospheric Radiation*, edited by W. L. Smith and Y. M. Timofeyev, A. Deepak, Hampton, Va., 2000.

Stowe, L. L., H. Y. M. Yeh, T. F. Eck, C. G. Wellemeyer, H. L. Kyle, and the Nimbus-7 Cloud Data Processing Team, Nimbus-7 global cloud climatology, Part II, First year results, *J. Clim.*, *2*, 671–709, 1989.

Vanbauce, C., J. C. Buriez, F. Parol, B. Bonnel, G. Sèze, and P. Couvert, Apparent pressure derived from ADEOS-POLDER observations in the oxygen A-band over ocean, *Geophys. Res. Lett.*, *25*, 3159–3162, 1998.

Winker, D. M., and C. R. Trepte, Laminar cirrus observed near the tropical tropopause by LITE, *Geophys. Res. Lett.*, *25*, 3351–3354, 1998.

J. F. de Haan and J. W. Hovenier, Department of Physics and Astronomy, Free University, De Boelelaan 1081, 1081 HV Amsterdam, Netherlands. (haandej@knmi.nl; hovenier@nat.vu.nl)

R. B. A. Koelemeijer, Air Research Laboratory, RIVM, P. O. Box 1, 3720 BA Bilthoven, Netherlands. (robert.koelemeijer@rivm.nl)

P. Stammes, Royal Netherlands Meteorological Institute, P. O. Box 201, 3730 AE De Bilt, Netherlands. (stammes@knmi.nl)

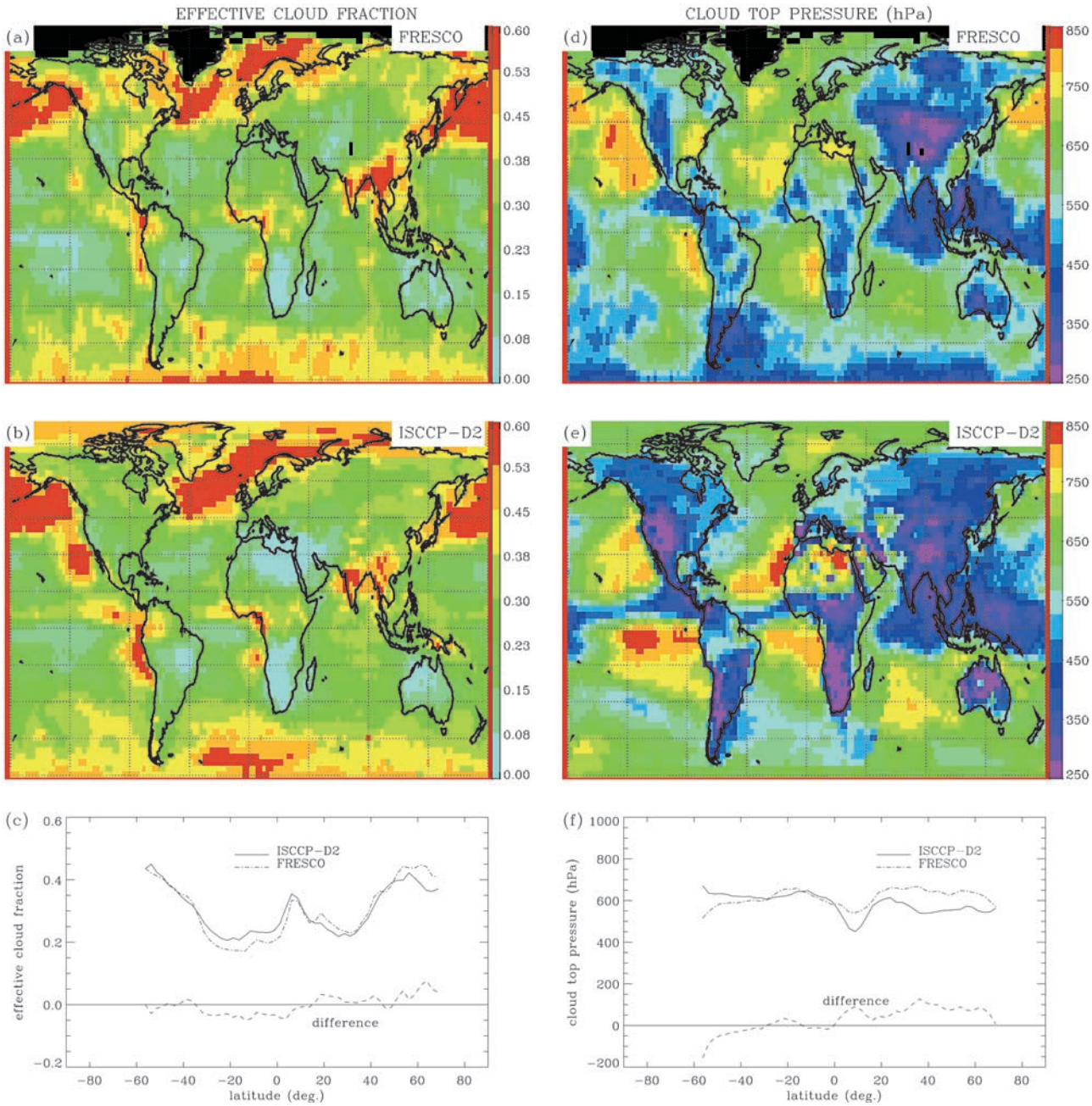

Figure 3. Monthly average effective cloud fractions and cloud top pressures of FRESCO and ISCCP. Effective cloud fractions are given for (a) FRESCO results, (b) ISCCP D2 results, and (c) zonal average; cloud top pressures (hectopascals) are given for (d) FRESCO results, (e) ISCCP results, and (f) zonal average. The FRESCO results are for July 1995, and the ISCCP results are July averages of 1989–1993.

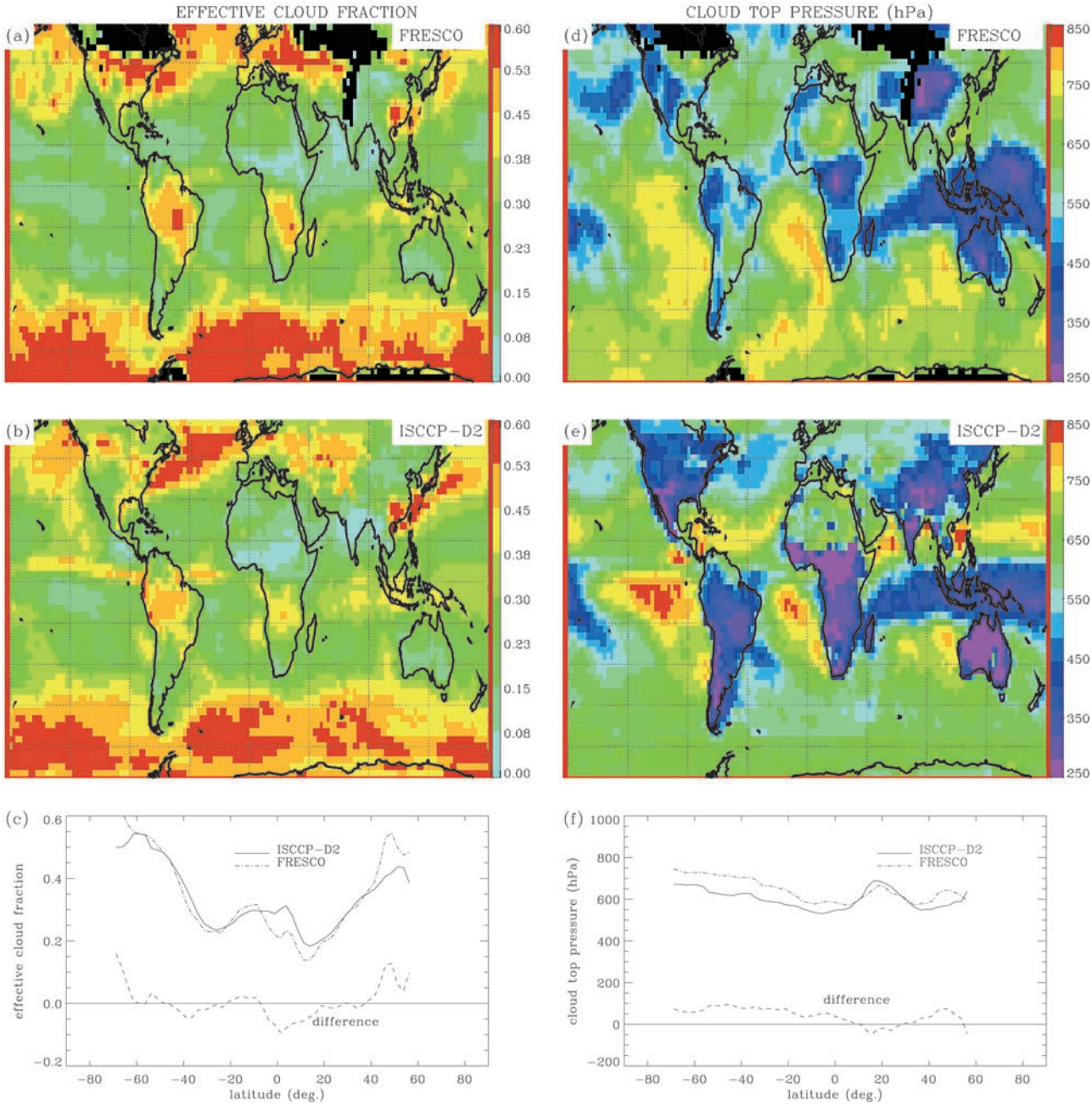

Figure 4. Same as Figure 3, but now the FRESCO results are for January 1997, and the ISCCP results are January averages of 1989–1993.